Original Article

Assessment of thoracic vasculature in patients with central bronchogenic carcinoma by unenhanced magnetic resonance angiography: comparison between 2D free-breathing TrueFISP, 2D breath-hold TrueFISP and 3D respiratory-triggered SPACE

Lili Wang[1,2], Peng Lv[1], Shuohui Yang[1], Mengsu Zeng[1], Jiang Lin[1,3]

[1]Department of Diagnostic Radiology, Shanghai Zhongshan Hospital, Shanghai Medical College of Fudan University and Shanghai Institute of Medical Imaging, Shanghai 200032, China; [2]Department of Radiology, Xiehe Hospital, Fujian Medical University, Fujian 350001, China; [3]Institute of Functional and Molecular Medical Imaging of Fudan University, Shanghai 200040, China

Contributions: (I) Conception and design: L Wang, J Lin; (II) Administrative support: None; (III) Provision of study materials or patients: L Wang, S Yang; (IV) Collection and assembly of data: P Lv, S Yang; (V) Data analysis and interpretation: L Wang, J Lin, P Lv, M Zeng; (VI) Manuscript writing: All authors; (VII) Final approval of manuscript: All authors.

Correspondence to: Jiang Lin. Department of Diagnostic Radiology, Shanghai Zhongshan Hospital, Shanghai Medical College of Fudan University and Shanghai Institute of Medical Imaging, Shanghai 200032, China. Email: lin.jiang@zs-hospital.sh.cn.

Background: Preoperative assessment of the integrity of major thoracic vessels in central bronchogenic carcinoma is vital for tumor staging and treatment planning. Contrast-enhanced CT is currently the first choice of modality for this purpose in clinical practice with limitations including exposure to ionizing radiation and the use of iodinated contrast material. MRI has been increasingly employed for the staging of lung cancer. More recently, unenhanced magnetic resonance angiography (MRA) which is totally non-invasive and contrast-free has been reported able to show thoracic vessels. This study was to compare image qualities of three unenhanced-MRAs and to evaluate accuracy of them in assessing thoracic vessel invasion by using contrast-enhanced CT as a reference standard.

Methods: A total of 30 patients with central bronchogenic carcinoma confirmed by pathology were examined by CT and unenhanced MRA including 2D free-breathing (FB)-TrueFISP, breath-holding (BH)-TrueFISP and 3D respiratory-triggered (RT)-SPACE. Image qualities of pulmonary arteries and veins, thoracic aorta and vena cava were scored for each MRA sequence. Vessel to lung tissue signal contrast-to-noise ratio (CNR), vessel to tumor signal contrast ratio (VTR), and tumor to background signal contrast ratio (TBR) were calculated. On each method, vessel invasion was evaluated according to types of morphological relationships between the tumor and major vessels.

Results: The three MRAs showed no significant difference in CNR (P=0.518) while TrueFISP MRAs were better than SPACE in terms of VTR (P=0.000) and image quality (P=0.002). Excellent consistency with CT was found for all three MRAs in assessment of the morphological relationships between tumors and major vessels (FB-TrueFISP: kappa =0.821; BH-TrueFISP: kappa =0.862; RT-SPACE: kappa =0.811).

Conclusions: Both TrueFISP and SPACE allow satisfactory visualization of major mediastinal and hilar vessels and are comparable to MDCT in assessment of vessel invasion in patients with central lung cancer. TrueFISP sequences are better than SPACE in regard to image quality and VTR.

Keywords: Bronchogenic carcinoma; magnetic resonance angiography (MRA); computed tomography (CT)

Submitted Feb 11, 2017. Accepted for publication May 16, 2017.
doi: 10.21037/jtd.2017.06.38
View this article at: http://dx.doi.org/10.21037/jtd.2017.06.38

Introduction

In patients with central bronchogenic carcinoma which located in segmental, lobar and main bronchus, preoperative assessment of the morphological relationship between tumor and mediastinal and hilar main vessels is considered important for disease staging and treatment planning. Invasion to large branches of pulmonary artery (PA) and vein, superior vena cava (SVC) and aorta can increase the difficulty of lung resection and therefore affects surgical resectability of the tumor (1). In addition, massive PA invasion is an indicator of worse prognosis for those patients (2).

The accuracy of contrast-enhanced multidetector row computed tomography (CE-MDCT) in evaluating tumor invasion of pulmonary vasculature and depicting anomalies of pulmonary arteries and veins has been investigated extensively and high sensitivity, and specificity have been confirmed (3,4). Meanwhile, magnetic resonance angiography (MRA) including contrast-enhanced and unenhanced MRA has been used as new techniques for assessing anomaly and tumor invasion of thoracic vessels without radiation (5,6). Both CE-MDCT and contrast-enhanced MRA use contrast media and are restricted in patients who had previous or potential adverse reactions to contrast media and in patients with significantly impaired renal function. Unenhanced MRA could be an option for safe and effective imaging in these patients especially, who need repeated follow-up studies.

Many studies have employed the steady-state free precession (SSFP) sequence and the sampling perfection with application-optimized contrasts using different flip angle evolutions (SPACE) sequence for imaging the PA, thoracic aorta and central veins and validated that they are very robust and reliable for diagnosing patients with pulmonary embolism, pulmonary vessel anomaly, aortic dissection and central venous pathology (7-9). However, little work has been done so far to systematically evaluate and compare these unenhanced MRA techniques in demonstration of the morphological relationship between lung cancer and mediastinal and hilar vessels. Hence the first objective of our study was to quantitatively and qualitatively evaluate and compare image qualities of three unenhanced MRA sequences including 2D free-breathing (FB) true fast imaging with SSFP (TrueFISP), breath-holding (BH) TrueFISP, and respiratory-triggered (RT) 3D T2-weighted SPACE sequence for demonstration of mediastinal and hilar vessels in patients with central lung cancer. The second objective was to evaluate accuracy of these three MRAs in evaluation of the relationship between the tumors and the vessels by using CE-MDCT as a reference standard.

Methods

Patients

Our study was approved by the institutional review board and written informed consent was obtained. Thirty consecutive patients [17 men and 13 women; mean age, 59 (range, 41–73) years] with a confirmed diagnosis of central lung cancer on the basis of CE-MDCT and bronchoscopy underwent chest MRI within an interval of 5 days after CT.

Eight cases of them were squamous cell carcinoma, 15 cases were adenocarcinoma and 7 cases were small cell lung cancer. All patients were examined by CE-MDCT, unenhanced FB-TrueFISP, BH-TrueFISP and RT-SPACE. The locations of lung cancers were as follows: right upper lobe in four patients, right lower lobe in six patients, left upper lobe in eight patients, left lower lobe in six patients, right middle lobe in one patient, and bilateral hilar regions involving multiple lobes in five patients.

Based on MDCT, thirteen patients with preoperative staging of I–III tumor subsequently underwent surgical resection within 10 days after MRI. Surgical procedures were video-assisted thoracoscopic (VATS) lobectomy in four patients, conventional lobectomy in eight patients and trans-bronchoscopic right intra-bronchial tumor ablation in one patient. The remaining 17 patients with tumors staged III–IV or with small cell lung cancer were treated by chemotherapy.

Contrast-enhanced MDCT

MDCT scans for chest were performed on a 16-detector row CT scanner (Lightspeed; GE Healthcare, Milwaukee, USA) with the following parameters: tube voltage, 120 kV; tube current, 200 mA; pitch, 1; matrix, 512 mm × 512 mm; field of view (FOV), 230 mm × 230 mm; section thickness, 0.625 mm. Image acquisition was performed 45 seconds after the administration of 80 mL contrast medium (Omnipaque; 300 mg I/mL; GE Healthcare) with 20 mL saline flush through an antecubital vein at an injection rate of 3 mL/sec by using a power injector (MALLINCKRODT, OptiVantage TM DH, USA).

MR imaging

All MR imaging examinations were performed on a 1.5-T

clinical MRI system (MAGNETOM Aera, Siemens Healthcare, Erlangen, Germany), using a body coil for transmission, and an 18-channel body array coil together with a 12-channel spine array coil for reception. Patients were examined in the supine position with their arms at two sides.

The FB and BH TrueFISP images were acquired in the coronal plane with the same following parameters: echo time (TE), 1.26 msec; echo spacing, 2.9 msec; flip angle, 70 degree; FOV, 380 mm × 380 mm; phase oversampling, 30%; matrix size, 256×256; slice thickness, 4.5 mm; slice distance factor, –60%, gap, –2.7 mm; a total of 128 slices were acquired; voxel size, 0.7 mm × 0.7 mm × 4.5 mm; 1 signal average; and bandwidth, 1,028 Hz per pixel. The different parameters between the two sequences were as follows: repetition time (TR), 559 msec for FB-TrueFISP and 407 msec for BH-TrueFISP; GRAPPA with parallel imaging acceleration factor, two for FB-TrueFISP and three for BH-TrueFISP; scanning times, 72 seconds for FB-TrueFISP and 56 seconds for BH-TrueFISP (twice BHs with 18-second each and a 20-second interval in-between).

SPACE sequence without blood suppression was performed in coronal plane with mean acquisition time of 3 minutes 25 seconds depending on the respiratory frequency of the patients. Protocol parameters are as follows: TR, variable (one respiration interval) with a mean time of 2,200 ms; TE, 102 msec; TI, 180 msec for fat suppression; echo spacing, 3.64 msec; flip angle of 150 degrees (constant mode); FOV, 380 mm × 285 mm; matrix size, 320×230; slice thickness, 4.5 mm; voxel size, 1.2 mm× 1.2 mm × 4.5 mm; GRAPPA with parallel imaging acceleration factor of three; two signal averages; bandwidth, 651 Hz/pixel; echo-train duration, 379 ms and turbo factor, 150.

Image analysis

Main trunks and branches of PA and vein, thoracic aorta, SVC and inferior vena cava (IVC) were assessed (*Table 1*). Two reviewers were asked to perform qualitative and quantitative image analysis separately on each sequence used for detection of those vessels in all 30 cases. Source images of the three different MRA sequences were independently analyzed by the two radiologists in random order.

First, qualitative analysis of the image quality was performed with regard to demonstration of vessels listed in *Table 1*. According to image grading standards proposed by Ohno *et al.* (6) and our own experience, a three point scale scoring system for image quality evaluation was used. Criteria were as follows: rank 1, good: the edge of the vasculature was clear, none artifacts were found; rank 2, average: the edge of the vasculature was clear or slightly blurring, minor artifacts were found, not affecting a diagnostic evaluation; rank 1 and 2 were considered adequate for diagnosis; rank 3, unsatisfactory and inadequate for diagnosis: the edge of the vasculature was blurring, major artifacts were found, substantially affecting a diagnostic evaluation. The image quality score for each patient was calculated from the average score of all the 20 vessels listed in *Table 1*.

Secondly, quantitative assessment of image quality was done by measuring vessel to lung signal contrast-to-noise ratio (CNR), vessel to tumor signal contrast ratio (VTR), and tumor to background signal ratio (TBR). The signal intensities (SI) and standard deviations (SD) were measured by drawing an ovoid region of interest (ROI) within the lumen of the target thoracic vessels as large as possible without including the vessel wall. Background signal intensity was measured in the ROI (range from 10 to 20 mm^2) in normal peripheral lung parenchyma avoiding lung vessels. Tumor signal intensity was measured in the ROI contouring the border of the lung cancer (avoiding necrosis) at the level showing longest diameter of the tumor on the coronal plane. The CNR, VTR and TBR were calculated from SI measurements on the MRA source images obtained with different techniques: CNR = (SI Vessel – SI Background)/SD Vessel; VTR = (SI Vessel – SI Tumor)/(SI Vessel + SI Tumor); TBR = (SI Tumor – SI Background)/(SI Tumor + SI Background).

Thirteen major mediastinal and hilar vessels that may affect surgical procedures were assessed. They were pulmonary arterial trunk, the right and left main PA, the right interlobar artery, the right upper lobe truncus anterior artery, the left upper lobe artery, the left lower lobe PA, the right and left superior and inferior pulmonary vein, the SVC and the aorta. Tumor invasion to these vessels was evaluated by different reviewers using image review software (3D, Siemens Healthcare, Erlangen, Germany). CE-MDCT images were reviewed by two radiologists with 28- and 5-year experience in body imaging. The reviewers were firstly asked to provide a detailed recording of the morphological relationship between the tumor and the thoracic vessels independently and secondly to make a consensus on vessel invasion and the final result was used as a standard reference for the following MRA prediction. Two other radiologists with 25 and 5 years of experience in body imaging independently reviewed all the three MRA sequences from these patients in a blinded fashion on

Table 1 Comparison of mean CNR[a] from three MRA sequences for each vessel

Variables	FB TrueFISP (S1)	BH TrueFISP (S2)	RT SPACE (S3)	Kruskal-Wallis H Test P value[b]	Wilcoxon-Signed rank Test P value[c]		
				S1–S2–S3	S1–S2	S1–S3	S2–S3
PA trunk	13.49±3.83	12.60±5.80	17.15±2.70	0.014*	0.353	0.029*	0.007*
Right PA							
Right main	13.94±1.23	14.87±5.02	19.39±9.06	0.490	0.436	0.393	0.393
Truncus anterior	16.34±9.33	11.29±3.25	15.40±6.92	0.348	0.247	0.971	0.218
Interlobe	18.23±4.05	17.93±5.54	16.12±2.38	0.478	0.529	0.190	0.912
Upper lobe branch	7.69±2.01	7.06±3.79	6.50±6.02	0.065	0.247	0.019*	0.315
Middle lobe branch	7.99±2.83	9.71±5.03	11.91±6.55	0.412	1.000	0.105	0.631
Lower lobe branch	8.72±5.84	7.46±1.56	7.84±3.32	0.961	0.796	0.971	0.912
Left PA							
Left main	17.88±3.98	16.55±4.02	19.31±5.14	0.460	0.579	0.631	0.218
Upper lobe	18.13±6.15	15.17±4.50	19.34±10.50	0.492	0.393	1.000	0.071
Lower lobe	22.87±3.49	16.92±6.74	17.19±6.59	0.072	0.023*	0.043*	0.796
Upper division branch	7.90±4.81	8.24±4.89	6.50±3.22	0.657	0.912	0.353	0.631
Lingular division branch	7.18±2.86	5.84±1.87	7.74±2.12	0.138	0.280	0.436	0.052
Lower lobe branch	6.15±1.89	8.68±2.81	7.15±3.69	0.068	0.023*	0.529	0.123
PV							
Right superior PV	14.49±6.81	14.70±4.77	15.33±8.90	0.772	0.631	0.912	0.529
Right inferior PV	14.63±5.80	14.51±11.19	13.23±6.40	0.939	0.739	0.853	1.000
Left superior PV	11.51±3.72	11.21±6.25	15.59±5.41	0.131	0.481	0.123*	0.089
Left inferior PV	10.39±6.24	5.99±1.87	6.86±2.95	0.312	0.190	0.247	0.739
Superior vena cava	13.73±4.65	10.85±4.43	24.31±11.24	0.007*	0.143	0.023*	0.004*
Inferior vena cava	7.12±2.22	8.73±3.76	13.04±5.34	0.014*	0.315	0.002*	0.105
Aorta	15.72±3.45	13.29±3.97	23.88±8.07	0.001*	0.123	0.003*	0.000*

[a], Data are means ± SD; [b], P value for FB-TrueFISP *vs.* BH-TrueFISP *vs.* RT-SPACE; [c], P value for FB-TrueFISP *vs.* BH-TrueFISP; FB-TrueFISP *vs.* RT-SPACE; BH-TrueFISP *vs.* RT-SPACE; *, Statistically significant difference was achieved when P<0.05. MRA, magnetic resonance angiography; FB, free-breathing; BH, breath-holding; RT, respiratory-triggered; PA, pulmonary artery; PV, pulmonary vein; CNR, signal contrast-to-noise ratios.

separate days with a minimum interval of 48 hours between reading sessions of different sequences. A consensus was reached between the two radiologists and used as a final determination.

Patterns of vessel invasion were defined and modified according to the reference of standard used by Han *et al.* (2), Herman *et al.* (10) and our own experience on post-processed coronal MRA: type 1, tumor-to-vessel distance >5 mm; type 2, 1–5 mm from the vessel wall, both types with preserved fat plane or normal lung between tumor and vasculature; type 3, direct tumor contact with one side of the vessel with smooth vessel wall and without vessel wall damage (irregularity or discontinuity) or narrowing or interruption of vessels; type 4, tumor contact with both sides of the vessel without vessel wall damage or narrowing or interruption of vessels; type 5, tumor contact with vessel wall damage or vascular narrowing but without vascular occlusion; type 6, vascular occlusion with or without displacement of the vessel by the tumor.

Statistical analysis

SPSS 17.0 for Windows (SPSS, Chicago, IL, USA) was used to perform all data analysis. All reported P values were exact two-sided and the significance level was set at 0.05 for all tests.

For image quality scoring and CNR, VTR and TBR

Table 2 Comparison of mean CNR[a], VTR[a], TBR[a] and image quality score[a] from two observers for all 20 target vessels

Variables	FB TrueFISP (S1)	BH TrueFISP (S2)	RT SPACE (S3)	Kruskal-Wallis H test P value[b]	Wilcoxon-Signed rank test P value[c]		
				S1–S2–S3	S1–S2	S1–S3	S2–S3
CNR	10.59±6.45	9.65±5.60	11.82±6.52	0.518	0.620	0.591	0.231
VTR	0.55±0.07	0.54±0.07	0.22±0.10	0.000*	0.561	0.000*	0.000*
TBR	0.81±0.04	0.80±0.05	0.83±0.06	0.035*	0.425	0.068	0.014*
Image quality score	1.23±0.35	1.24±0.29	1.37±0.42	0.002*	0.056	0.001*	0.015*

[a], Data are means ± SD; [b], P value for FB-TrueFISP *vs.* BH-TrueFISP *vs.* RT-SPACE; [c], P value for FB-TrueFISP *vs.* BH-TrueFISP; FB-TrueFISP *vs.* RT-SPACE; BH-TrueFISP *vs.* RT-SPACE; *, statistically significant difference was achieved when P<0.05. FB, free-breathing; BH, breath-holding; RT, respiratory-triggered; CNR, signal contrast-to-noise ratios; VTR, vessel-to-tumor contrast ratios; TBR, tumor-to-background contrast ratios.

on each of the three MRA sequences, the mean values of the two readers were calculated. A nonparametric Kruskal-Wallis H test was used to compare the diversity of these values from three MRA sequences, and then a Wilcoxon-signed rank test was used for further pairwise comparison of the difference between any two of the three sequences.

For prediction of vessel invasion by the tumor, the final results achieved by the two readers in consensus were used. Kappa statistics was used to compare the consistency between each of the three MRA sequences and CE-MDCT examination for the type of morphological relationship between the tumors and vessels. The consistency was considered as poor, when kappa <0.5; moderate, when kappa =0.5–0.8; and excellent, when kappa >0.8.

For the level of the agreement between the two reviewers, an intraclass coefficient was used for the measurement of CNR, VTR and TBR and ak coefficient was estimated as a measurement for image quality scoring and the type of the morphological relationship between the tumor and the vessels. Interobserver agreement was considered as poor when r or kappa was <0.5, moderate when r or kappa was 0.5–0.8 and excellent when r or kappa was >0.8.

Results

All unenhanced MRA examinations were successfully performed in 30 patients. Results of the image quality score and CNR, VTR and TBR from the three MRA sequences were summarized in *Tables 1* and *2*. Regarding CNR, there was no significant difference among these MRAs. However, VTR and image quality on both TrueFISP sequences were better than those on SPACE while TBR on SPACE was better than that on BH-TrueFISP. Image quality from all 30 patients was scored adequate for diagnosis on both TrueFISP and SPACE sequences. A pseudo-filling defect in SVC was found on BH-TrueFISP in two patients probably owing to the increased intrathoracic pressure during BH, however this did not interfere with the diagnosis.

Table 3 summarized the results of the morphological relationship between tumors and the vessels observed on each of the MRAs on a per-technique basis, taking into account 13 major mediastinal and hilar vessels, with MDCT findings being used as the reference standard. All the three MRA sequences showed excellent consistency with CE-MDCT in assessment of the relationship between tumors and vessels (FB-TrueFISP: kappa =0.821; BH-TrueFISP: kappa =0.862; RT-SPACE: kappa =0.811) (*Figure 1*). All the inconsistencies between TrueFISP and MDCT were found in pulmonary arterial and venous branches, but none in SVC and aorta. There were two of the inconsistencies between SPACE and MDCT present in SVC, others were located in pulmonary arterial and venous branches.

There were moderate to excellent agreements between the two readers for CNR measurements (FB-TrueFISP: r=0.814; BH-TrueFISP: r=0.812; RT-SPACE: r=0.768), VTR (FB-TrueFISP: r=0.786; BH-TrueFISP: r=0.839; RT-SPACE: r=0.872) and TBR measurements (FB-TrueFISP: r=0.754; BH-TrueFISP: r=0.864; RT-SPACE: r=0.871). Excellent consistency was achieved between the two readers for image quality scoring (FB-TrueFISP: k=0.832, BH-TrueFISP: k=0.886, RT-SPACE: k=0.907) and predicting the type of morphological relationship between tumors and vessels (FB-TrueFISP; k=0.918, BH-TrueFISP; k=0.984, RT-SPACE; k=0.901, MDCT; k=0.936) (*Table 4*).

Discussion

Time-of-flight (TOF) and phase-contrast (PC) are two most

Table 3 Number of vessels from three MRA sequences and contrast-enhanced MDCT showing different morphological relationship type between tumors and vessels

Variables	MDCT							Kappa value[a] (k)
	1	2	3	4	5	6	Total	
FB TrueFISP								
1[b]	334	0	0	0	1	0	335	
2[b]	0	2	3	0	2	0	7	
3[b]	0	2	11	0	0	0	13	
4[b]	0	0	0	5	5	0	10	
5[b]	0	0	0	4	18	0	22	
6[b]	0	0	0	0	1	2	3	
Total	334	4	14	9	27	2	390[c]	0.821
BH TrueFISP								
1	334	0	0	0	0	0	334	
2	0	2	2	0	1	0	5	
3	0	2	12	0	2	0	16	
4	0	0	0	6	2	0	8	
5	0	0	0	3	20	0	23	
6	0	0	0	0	2	2	4	
Total	334	4	14	9	27	2	390	0.862
RT SPACE								
1	334	0	0	0	1	0	335	
2	0	1	3	0	0	0	4	
3	0	3	11	2	3	0	19	
4	0	0	0	3	0	0	3	
5	0	0	0	4	20	0	24	
6	0	0	0	0	3	2	5	
Total	334	4	14	9	27	2	390	0.811

[a], Kappa test for the consistency between each of the three MRA sequences and the MDCT; [b], morphological relationship between the tumors and vessels; [c], a total of 390 vessels from 30 patients were assessed in regard to the morphological relationship between tumors and vessels. FB, free-breathing; BH, breath-holding; RT, respiratory-triggered; MRA, magnetic resonance angiography.

commonly used unenhanced MRA techniques, however, they are time consuming and prone to in-plane saturation and flow artifacts leading to signal loss or overestimation of vessel stenosis. On the contrary, both TrueFISP and 3D SPACE MRA are flow independent sequences with high signal-to-noise ratio for vessels. Additionally tumors on these sequences can be visualized simultaneously, providing the potential for showing the morphological relationship between vessels and tumors. Furthermore coronal acquisition used in our study is useful in demonstrating the extent of the tumor involving the aorto-pulmonary window, and SVC (11) and allowed larger longitudinal coverage in a shorter scanning time.

In this study, the image quality of the three MRAs was evaluated by CNR and image quality scoring. Overall, when all patients were taken into account regardless of the vessel segments, no significant difference in the CNR was found among the three unenhanced MR sequences. But image

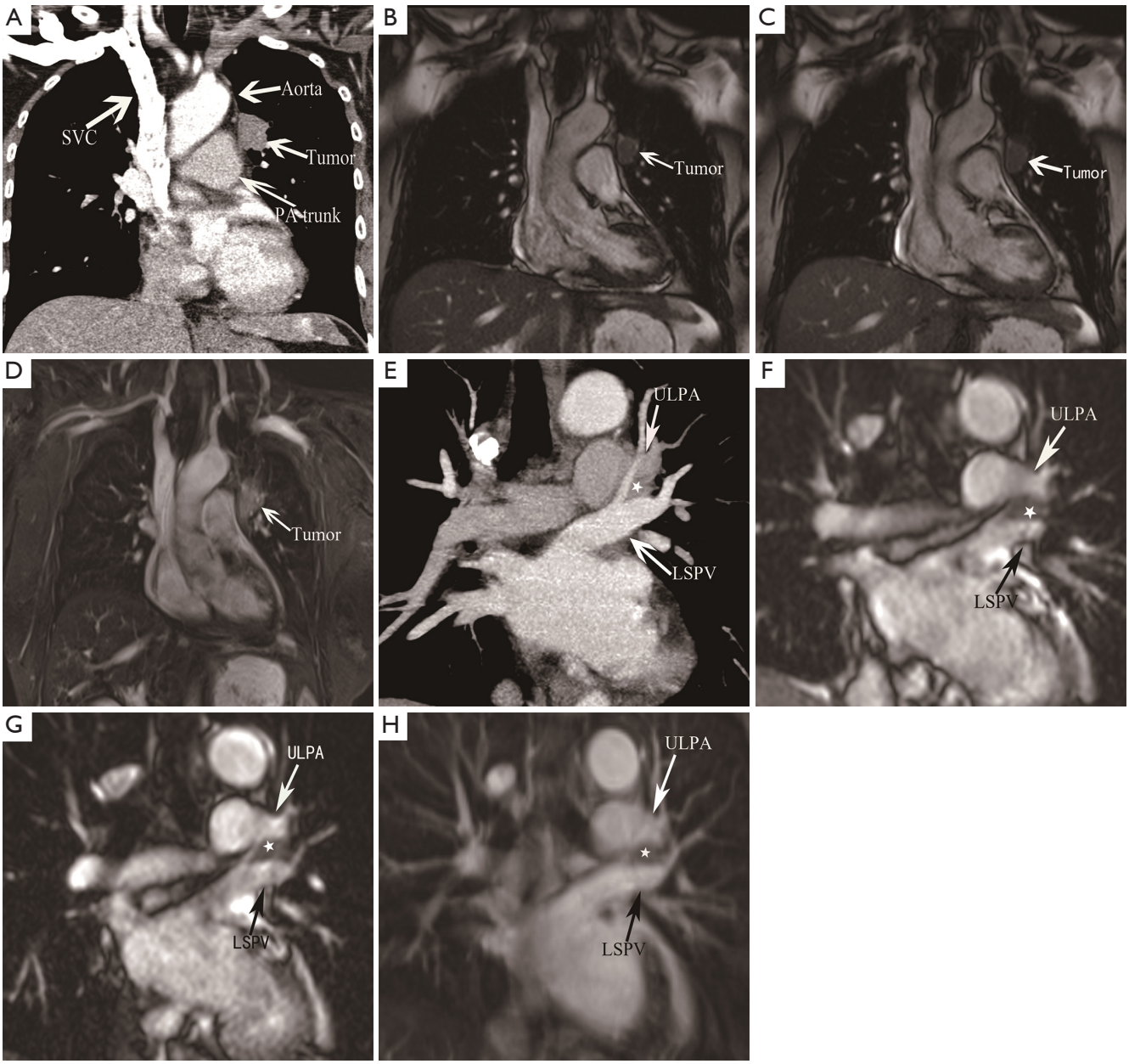

Figure 1 A 52-year-old woman with central lung adenocarcinoma located in the left upper lobe. Coronal slices from CE-MDCT (A), FB-TrueFISP (B), BH-TrueFISP (C) and RT-SPACE (D) show type 1 relationship between the tumor and aorta, and type 2 relationship between the tumor and pulmonary artery trunk (PA trunk). More posteriorly coronal slices from CE-MDCT (E), FB-TrueFISP (F), BH-TrueFISP (G) and RT-SPACE (H) show type 3 relationships between the tumor (asterisk) and left ULPA and LSPV. TrueFISP shows better vessel to tumor contrast than SPACE. Left upper lobe lobectomy was performed and invasion to the aorta, pulmonary artery trunk, left ULPA and superior pulmonary vein was not found at surgery. CE-MDCT, contrast-enhanced multidetector row computed tomography; FB, free-breathing; BH, breath-holding; RT, respiratory-triggered; PA, pulmonary artery; ULPA, upper lobe pulmonary artery; LSPV, left superior pulmonary vein.

Table 4 Interobserver agreement for predicting morphological relationship between the tumor and vessels in three MRA sequences and CE-MDCT

Imaging modality/observer	Morphological relationship type						Kappa value[b] (k)
	1	2	3	4	5	6	
FB TrueFISP							
Observer 1	335	8	13	11	20	3	
Observer 2	335	6	14	8	24	3	0.918
Final decision[a]	335	7	13	10	22	3	
BH TrueFISP							
Observer 1	334	5	16	8	24	3	
Observer 2	334	5	16	8	22	5	0.984
Final decision	334	5	16	8	23	4	
RT SPACE							
Observer 1	335	3	19	4	26	3	
Observer 2	335	6	18	2	22	7	0.901
Final decision	335	4	19	3	24	5	
CE-MDCT							
Observer 1	334	4	14	9	27	2	
Observer 2	334	4	14	8	27	3	0.936
Final decision	334	4	14	9	27	2	

[a], final decision was made by both two observers in consensus; [b], kappa test for the interobserver agreement between observer 1 and observer 2. MRA, magnetic resonance angiography; FB, free-breathing; BH, breath-holding; RT, respiratory-triggered; CE-MDCT, contrast-enhanced multidetector row computed tomography.

quality scoring in TrueFISP sequences was better than that in SPACE. All the three MRA sequences showed excellent agreement with MDCT in assessment of the morphological relationship between the lung cancer and the neighboring thoracic vessels.

The 3D turbo spin echo (TSE)-based SPACE enables acquisition of a volumetric T2-weighted data set with long echo train. Although variable flip angle is one of important advantages of SPACE sequence, constant flip angle mode with 150 degrees was used in our study. With this mode, higher SNR and better contrast can be achieved for both vessels and lesion visualization. Non-selective excitation and non-selective refocusing RF pulses were used in this sequence, which made very short echo spacing, short echo-train duration and less T2 blurring possible. SPACE sequence can also mitigate flow and motion artifacts, prevent inflow effects and allow for signal contrast between different tissues to emerge (12). In recent studies, 3D SPACE sequence has been used for imaging of lower peripheral artery (13), central veins of the chest (9) and portal veins (14) with improved spatial resolution and speed. Since it is the relaxation properties of blood rather than flow that generate the signal contrast, the SPACE sequence can guarantee the visualization of the vessels and presence of stenosis and occlusion (9). This capability was further confirmed by our study in demonstration of vascular integrity in patients with lung cancers.

SSFP technique is a revolutionary technique in unenhanced MRA for excellent evaluation of blood vessels owing to its relatively short imaging time, high vessel signal-to-noise ratio and uniform contrast between blood and the adjacent tissue (15,16). In recent studies, balanced SSFP, or called TrueFISP, has been used in cardiovascular imaging. TrueFISP has demonstrated high specificity for evaluation of pulmonary embolism (17). Compared to contrast-enhanced MRA, high image quality, high SNR and CNR were found in imaging of different target vessels (18-20). Studies also showed that SSFP sequence was accurate in measurements of diameters of PA and veins (21-23). In our study, both FB and BH TrueFISP sequences showed good image quality of the mediastinal and hilar vessels and high accuracy in assessment of the morphological relationship

between tumors and vessels.

Unenhanced MRA would be vulnerable to cardiac motion artifact, especially patients with arrhythmia, inducing both image quality deterioration and assessment of vascular invasion more difficult (24). Furthermore, relatively bigger voxel size and lower VTR in our SPACE sequence could lead to its inferior image quality and misinterpretation of vessel invasion because of the partial volume effect. Compared to SPACE, TrueFISP is a single-shot acquisition allowing FB or even BH imaging. TrueFISP can be acquired with better spatial resolution resulted from slice overlapping and has better vessel to tumor contrast than SPACE. These factors contributed to improved consistency between TrueFISP and MDCT in assessment of the relationship between the tumor and the vessels.

One limitation of our study is that MDCT, rather than the surgery and pathology results, was considered as the reference standard in assessment of vessel invasion, because many patients with central lung cancer were not eligible for surgery and contrast-enhanced MDCT has been a well-established and reliable method in evaluation of tumor invasion into the blood vessels. Another limitation is that TrueFISP with respiratory triggering which has been introduced as an effective method for vascular imaging was not done because of its relatively longer scanning time. Thirdly, electrocardiographic (ECG) triggering with data acquisition was not applied to these unenhanced MRAs to minimize cardiac motion artifacts because it would further increase scanning time. Unlike MDCT, both TrueFISP and SPACE were acquired in coronal plane in order to shorten the scan time. Although the source images from unenhanced MRA could be reformatted into any plane to better evaluate the vessel invasion, their spatial resolution would be sacrificed in doing so owing to anisotropic nature of MRA. A direct comparison with contrast-enhanced MRA was considered but hampered by the fact that patients' expenditure and contrast load would increase. Finally, the study was conducted in only one medical center and the sample size was relatively small and therefore studies with larger patient population are needed in the future.

In summary, our study demonstrated that unenhanced MRA based on TrueFISP and SPACE allowed adequate visualization of major mediastinal and hilar vessels and was comparable to CE-MDCT in assessment of the vessel invasion in patients with central bronchiogenic carcinoma. Both TrueFISP sequences are better than SPACE in terms of image quality and vessel to tumor contrast. These unenhanced MRA sequences which do not use contrast media and are free from radiation may be considered as options in depiction of vessel integrity in these patients.

Acknowledgements

None.

Footnote

Conflicts of Interest: The authors have no conflicts of interest to declare.

Ethical Statement: The study was approved by the Institutional Review Board of the hospital (No. B2014127) and written informed consent was obtained from all patients.

References

1. Xuegang L, Chao S, Zhen T, et al. Pulmonary artery Reconstruction using autologous pericardium or azygos venae substitute for surgical treatment of central non-small cell lung cancer. Cell Biochem Biophys 2013;67:949-55.
2. Han CB, Wang WL, Quint L, et al. Pulmonary artery invasion, high-dose radiation, and overall survival in patients with non-small cell lung cancer. Int J Radiat Oncol Biol Phys 2014;89:313-21.
3. Higashino T, Ohno Y, Takenaka D, et al. Thin-section multiplanar reformats from multidetector-row CT data: utility for assessment of regional tumor extent in non-small cell lung cancer. Eur J Radiol 2005;56:48-55.
4. Fukuhara K, Akashi A, Nakane S, et al. Preoperative assessment of the pulmonary artery by three-dimensional computed tomography before video-assisted thoracic surgery lobectomy. Eur J Cardiothorac Surg 2008;34:875-7.
5. Ohno Y, Nishio M, Koyama H, et al. Journal Club: Comparison of assessment of preoperative pulmonary vasculature in patients with non-small cell lung cancer by non-contrast- and 4D contrast-enhanced 3-T MR angiography and contrast-enhanced 64-MDCT. AJR Am J Roentgenol 2014;202:493-506.
6. Ohno Y, Adachi S, Motoyama A, et al. Multiphase ECG-triggered 3D contrast-enhanced Mr angiography: utility for evaluation of hilar and mediastinal invasion of bronchogenic carcinoma. J Magn Reson Imaging 2001;13:215-24.
7. Miyazaki M, Lee VS. Nonenhanced Mr angiography. Radiology 2008;248:20-43.
8. Miyazaki M, Akahane M. Non-contrast enhanced Mr

angiography: established techniques. J Magn Reson Imaging 2012;35:1-19.
9. Kim CY, Bashir MR, Heye T, et al. Respiratory-gated noncontrast SPACE MR angiography sequence at 3T for evaluation of the central veins of the chest: a feasibility study. J Magn Reson Imaging 2015;41:67-73.
10. Herman SJ, Winton TL, Weisbrod GL, et al. Mediastinal invasion by bronchogenic carcinoma: CT signs. Radiology 1994;190:841-6.
11. Bryant AS, Cerfolio RJ. Diagnosis, staging and treatment of patients with non-small cell lung cancer for the surgeon. Indian J Surg 2009;71:310-6.
12. Lichy MP, Wietek BM, Mugler JP, et al. Magnetic resonance imaging of the body trunk using a single-slab, 3-dimensional, T2-weighted turbo-spin-echo sequence with high sampling efficiency (SPACE) for high spatial resolution imaging: initial clinical experiences. Invest Radiol 2005;40:754-60.
13. Li D, Lin J, Yan F, et al. Unenhanced calf MR angiography at 3.0 T using electrocardiography-gated partial-fourier fast spin echo imaging with variable flip angle. Eur Radiol 2011;21:1311-22.
14. Song Q, Zeng MS, Chen CZ, et al. Non-Contrast-Enhanced magnetic resonance angiography using T2-Weighted 3-Dimensional Fat-Suppressed turbo spin echo (SPACE): diagnostic performance and comparison with Contrast-Enhanced magnetic resonance angiography using volume interpolated Breath-Hold examination in the detection of portosystemic and portohepatic collaterals. J Comput Assist Tomogr 2012;36:675-80.
15. Fuchs F, Laub G, Othomo K. TrueFISP--technical considerations and cardiovascular applications. Eur J Radiol 2003;46:28-32.
16. Krishnam MS, Tomasian A, Deshpande V, et al. Noncontrast 3D steady-state free-precession magnetic resonance angiography of the whole chest using nonselective radiofrequency excitation over a large field of view: comparison with single-phase 3D contrast-enhanced magnetic resonance angiography. Invest Radiol 2008;43:411-20.
17. Kalb B, Sharma P, Tigges S, et al. Mr imaging of pulmonary embolism: diagnostic accuracy of contrast-enhanced 3D Mr pulmonary angiography, contrast-enhanced low-flip angle 3D GRE, and nonenhanced free-induction FISP sequences. Radiology 2012;263:271-8.
18. Tomasian A, Lohan DG, Laub G, et al. Noncontrast 3D steady state free precession magnetic resonance angiography of the thoracic central veins using nonselective radiofrequency excitation over a large field of view: initial experience. Invest Radiol 2008;43:306-13.
19. Krishnam MS, Tomasian A, Malik S, et al. Image quality and diagnostic accuracy of unenhanced SSFP Mr angiography compared with conventional contrast-enhanced Mr angiography for the assessment of thoracic aortic diseases. Eur Radiol 2010;20:1311-20.
20. Raoult H, Gauvrit JY, Schmitt P, et al. Non-ECG-gated unenhanced MRA of the carotids: optimization and clinical feasibility. Eur Radiol 2013;23:3020-8.
21. Gadabanahalli K, Bhat V, Kumar P, et al. Implication of pulmonary-systemic flow information in the management of complex presentation of pulmonary arterial hypertension: exploring role of phase contrast MRI technique. Quant Imaging Med Surg 2017;7:276-80.
22. Shariat M, Schantz D, Yoo SJ, et al. Pulmonary artery pulsatility and effect on vessel diameter assessment in magnetic resonance imaging. Eur J Radiol 2014;83:378-83.
23. Groth M, Bannas P, Regier M, et al. Precision of pulmonary vein diameter measurements assessed by CE-MRA and steady-state-free precession imaging. Eur Radiol 2013;23:1546-52.
24. Rodrigues J, Minhas K, Pieles G, et al. The effect of reducing spatial resolution by in-plane partial volume averaging on peak velocity measurements in phase contrast magnetic resonance angiography. Quant Imaging Med Surg 2016;6:564-72.

Cite this article as: Wang L, Lv P, Yang S, Zeng M, Lin J. Assessment of thoracic vasculature in patients with central bronchogenic carcinoma by unenhanced magnetic resonance angiography: comparison between 2D free-breathing TrueFISP, 2D breath-hold TrueFISP and 3D respiratory-triggered SPACE. J Thorac Dis 2017;9(6):1624-1633. doi: 10.21037/jtd.2017.06.38

